Ammonia decomposition on Ir(100): from ultrahigh vacuum to elevated pressures

T.V. Choudhary, A.K. Santra, C. Sivadinarayana, B.K. Min, C.-W. Yi, K. Davis and D.W. Goodman *

Department of Chemistry, Texas A&M University, PO Box 30012, College Station, TX 77840, USA
E-mail: goodman@mail.chem.tamu.edu

Received 21 June 2001; accepted 7 August 2001

Ammonia decomposition on Ir(100) has been studied over the pressure range from ultrahigh vacuum to 1.5 Torr and at temperatures ranging from 200 to 800 K. The kinetics of the ammonia decomposition reaction was monitored by total pressure change. The apparent activation energy obtained in this study (84 kJ/mol) is in excellent agreement with our previous studies using supported Ir catalysts (Ir/Al_2O_3 82 kJ/mol). Partial pressure dependence studies of the reaction rate yielded a positive order (0.9 ± 0.1) with respect to ammonia and negative order (-0.7 ± 0.1) with respect to hydrogen. Temperature-programmed desorption data from clean and hydrogen co-adsorbed Ir(100) surfaces indicate that ammonia undergoes facile decomposition on both these surfaces. Recombinative desorption of N_2 is the rate-determining step with a desorption activation energy of ~63 kJ/mol. Co-adsorption data also indicate that the observed negative order with respect to hydrogen pressure is due to enhancement of the reverse reaction ($NH_x + H \rightarrow NH_{x+1}$, $x = 0$–2) in the presence of excess H atoms on the surface.

KEY WORDS: ammonia; CO_x-free; hydrogen production; decomposition; co-adsorption

1. Introduction

In recent years fuel cells have attracted considerable attention for energy generation because of their high efficiency and non-polluting nature. Low-temperature fuel cells require hydrogen free of CO for optimum operation; proton exchange membrane fuel cells can tolerate only ppm levels of CO in the hydrogen stream, whereas alkaline fuel cells require hydrogen free of CO_2. Conventional hydrogen production technologies such as steam reforming, partial oxidation and autothermal reforming of hydrocarbons result in the production of a large amount of CO_x as a by-product along with hydrogen [1,2]. Removal of CO_x to ppm levels from the hydrogen stream makes the process extremely complex and cumbersome, thereby prohibiting the use of existing hydrogen production technologies in vehicular and small-scale fuel cell applications. These limitations have motivated us to explore CO_x-free alternatives for hydrogen production for applications in fuel cells [3–6]. Recently we have proposed stepwise steam reforming of methane/hydrocarbons as a method for production of CO-free hydrogen [3,4]. An alternative approach involves the catalytic decomposition of ammonia and represents an extremely interesting route for hydrogen production, since no CO or CO_2 are formed; nitrogen is the only by-product. Moreover, theoretical calculations have shown ammonia decomposition to be an economically feasible process for fuel cell applications [7,8]. Decomposition of ammonia has been studied on a variety of transition metal single crystal surfaces [9–13]. In general it has been observed that although the early transition metals are very active toward ammonia decomposition, they either suffer from the relatively high recombinative desorption temperatures for N_2 (the step which has been recognized as the rate-determining step) or undergo deactivation due to nitride formation. On the other hand, late transition metals provide reasonable temperatures for the recombinative desorption of N_2 with moderate or low activity for decomposition itself. Studies on metal wires have shown that Ir is the most active catalyst for ammonia decomposition compared to Pd, Pt, Rh and Ni [14,15]. Ir catalysts dispersed on Al_2O_3 are also found to be most efficient and are commonly used in space propulsion for the decomposition of hydrazine in monopropellant thrusters [16]. To our knowledge there have been no studies in the literature concerning ammonia decomposition at Ir single crystal surfaces. Therefore, we have carried out kinetic measurements in a high-pressure reactor and TPD studies in UHV to understand the overall reaction mechanism.

2. Experimental

The experiments were carried out in two ultrahigh vacuum (UHV) chambers (base pressure $= 2 \times 10^{-10}$ Torr). The high-pressure experiments were carried out in a chamber contiguous with an elevated pressure reactor [17] whereas pre- and post-reaction surface analyses were accomplished in the UHV chamber by Auger electron spectroscopy (AES). The temperature-programmed desorption (TPD) experiments were carried out in a chamber equipped with X-ray photoelectron spectroscopy (XPS), AES, low-energy electron diffraction (LEED), and ion scattering spec-

* To whom correspondence should be addressed.

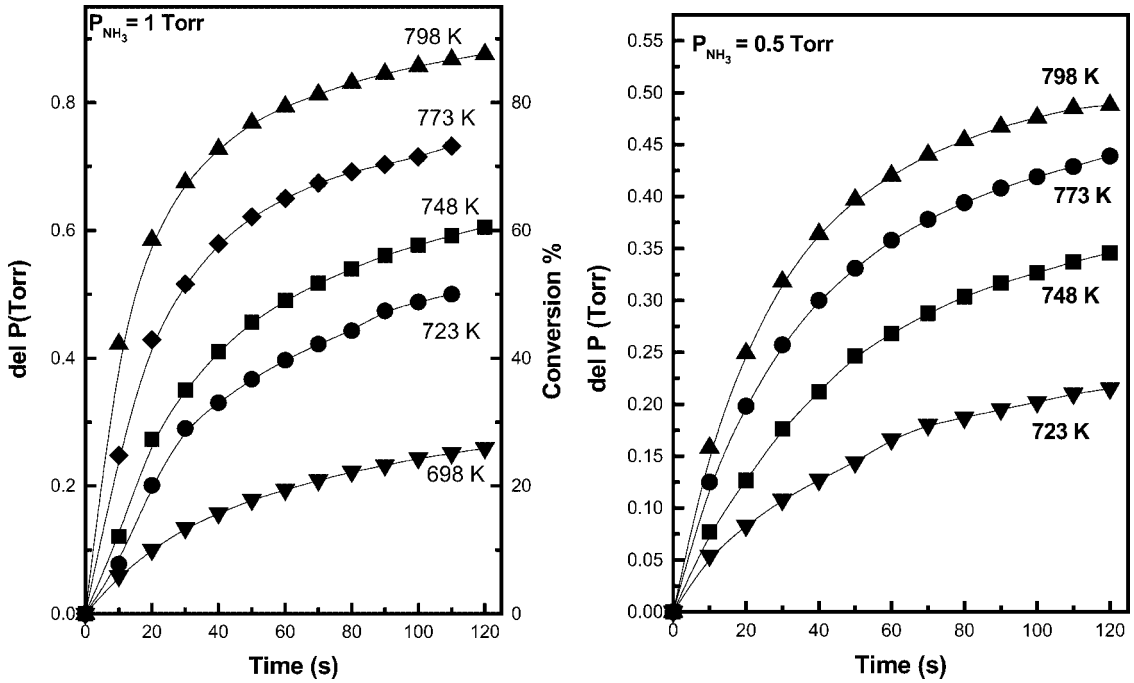

Figure 1. Total pressure change during ammonia decomposition on Ir(100) as a function of reaction time at initial ammonia pressures of (a) 1 and (b) 0.5 Torr.

troscopy (ISS) [18]. The Ir crystal was cleaned in UHV by occasional argon sputtering and repeated cycles of heating in O_2 ($P = 5 \times 10^{-7}$ Torr, 10 min) followed by annealing to 1600 K until no detectable C and O signals were obtained in AES. Anhydrous NH_3 (99.99%, Matheson) and $^{15}ND_3$ (Icon Isotopes, ^{15}N/99% and D/98%) was further purified by the freeze, pump and thaw method; hydrogen (99.999%, Matheson) was purified by passing through a liquid nitrogen trap. The crystal was mounted on a Ta sample holder (0.0255 cm diameter); temperature of the sample was monitored with a W–5%Re/W–26%Re thermocouple spot-welded to the back of the sample. TPD experiments were performed by a UT quadrupole mass spectrometer with a heating rate of 5 K/s.

Since dissociation of each ammonia molecule results in the formation of two product molecules ($NH_3 \rightarrow \frac{1}{2}N_2 + \frac{3}{2}H_2$), the pressure in the reaction cell (static reactor) will increase as the reaction proceeds. To follow the reaction the change in pressure was monitored as a function of time by a Baratron pressure gauge. Some ammonia was found to adsorb on the walls of the chamber when introduced to the elevated pressure reactor. The pressure change resulting from this adsorption was monitored as a function of time and the data corrected accordingly. The Ir(100) surface was heated (in the elevated pressure reactor) to the desired reaction temperature prior to introduction of ammonia and ammonia/hydrogen mixtures.

3. Results and discussion

Ammonia decomposition on Ir(100) was investigated in a temperature range of 700–800 K and a pressure range from 0.5 to 1.5 Torr. Figure 1 (a) and (b) shows the decomposition of ammonia with initial ammonia pressures of 1.0 and 0.5 Torr, respectively, at various reaction temperatures. The plots are B-spline fits and serve to guide the eye. A similar trend is observed in both cases; the decomposition rate increases linearly with time for the first few seconds, after which there is a slow gradual increase. Initial ammonia decomposition rates were obtained from the slopes of the linear portions of the plots. Figure 2 shows an Arrhenius plot for ammonia decomposition on Ir(100) at 1.0 Torr initial pressure of ammonia. An apparent activation energy (E_a) of 84 kJ/mol was obtained from the slope of the plot. This value is in excellent agreement with values found for am-

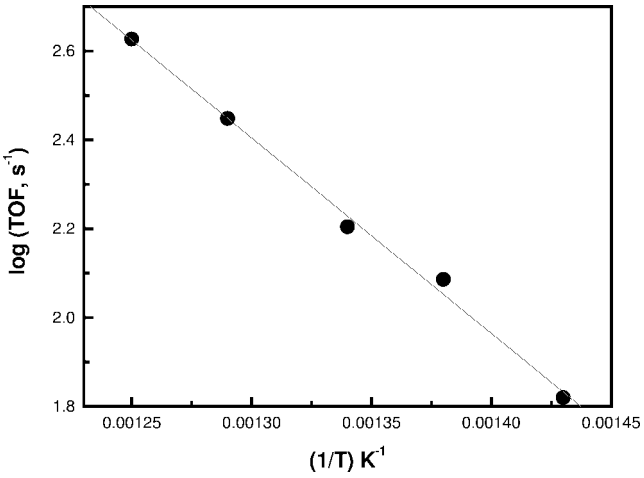

Figure 2. Arrhenius plot for ammonia decomposition on Ir(100) at $P(NH_3) = 1$ Torr.

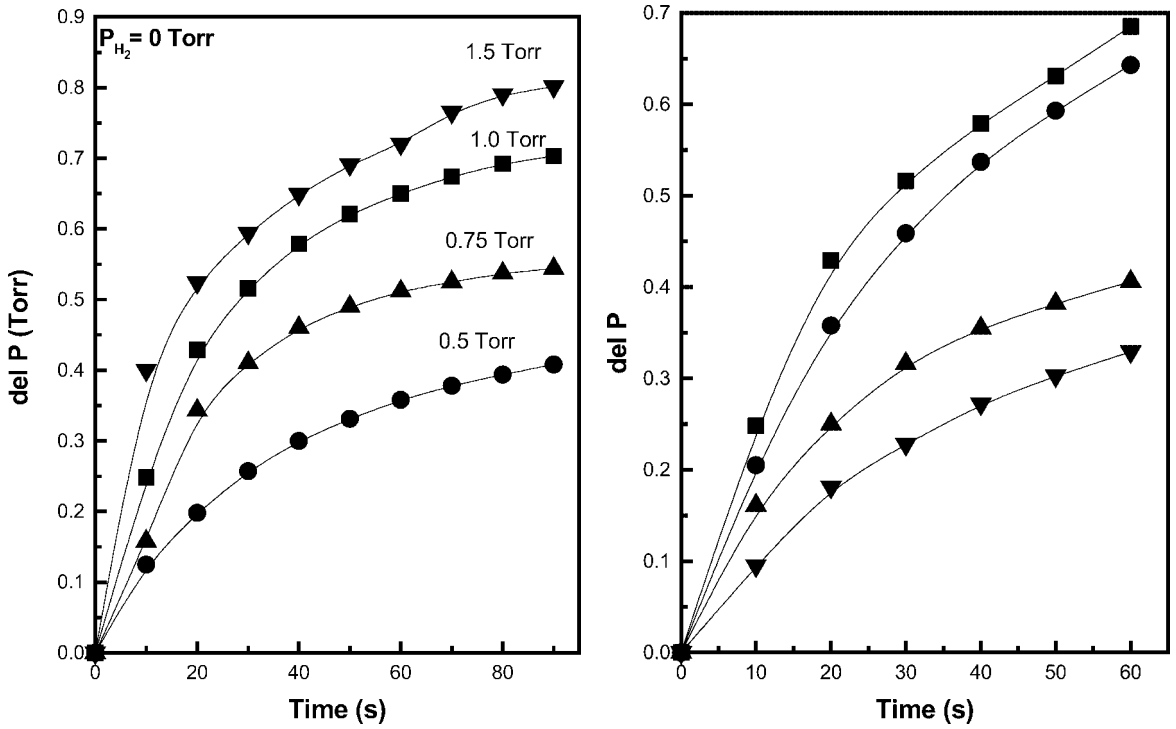

Figure 3. Total pressure change during ammonia decomposition on Ir(100) as a function of reaction time at (a) ammonia partial pressures of 0.5, 0.75, 1.0 and 1.5 Torr. $P(H_2) = 0$ and (b) hydrogen partial pressures of 0, 0.25, 0.5 and 1.0 Torr. $P(NH_3) = 1$ Torr, $T = 775$ K.

monia decomposition on real-world Ir/Al_2O_3 (∼82 kJ/mol) catalysts [19] and elsewhere in the literature [20], thereby implying that the reaction is probably structure insensitive. From figure 1 (a) and (b) it is apparent that with increasing reaction temperature the plots deviate from linearity at higher conversions of ammonia, likely due to the increased production of H_2 in the reaction mixture. It is also noteworthy that the percentage of ammonia conversion at the roll-over point increases with an increase in reaction temperature indicating that the actual dynamic coverage of hydrogen atoms produced by dissociation of H_2 and NH_3 (also dependent on the lifetime of the H atom on the surface which is a function of surface temperature) is likely an important factor to be considered in understanding the roll-over effect.

To check the effect of the partial pressure of hydrogen in the gas mixture we have performed kinetic measurements starting with an ammonia and hydrogen gas mixture. Figure 3 (a) and (b) shows the effect of ammonia and hydrogen partial pressures, respectively, on the rate of the ammonia decomposition reaction. In these experiments the total pressure change was monitored as a function of reaction time for different gas-mixture compositions at 773 K. The rate of the ammonia decomposition was found to increase with increasing partial pressures of ammonia (zero hydrogen partial pressure) while the rate was observed to decrease with increasing partial pressures of hydrogen (constant ammonia pressure of 1.0 Torr). The slopes of these plots were used to determine the ammonia and hydrogen partial pressure dependencies. These results are shown in figure 4, wherein the specific ammonia decomposition rates are plotted as a function of the partial pressures of the reactants in logarithmic forms. From the slopes of these plots we have calculated the order of the reaction to be 0.9 and −0.7 for ammonia and hydrogen, respectively. Recent ammonia decomposition studies on Ir wires [14] have shown the reaction to be independent of the partial pressure of ammonia at temperatures below 700 K and first order at temperatures above 700 K.

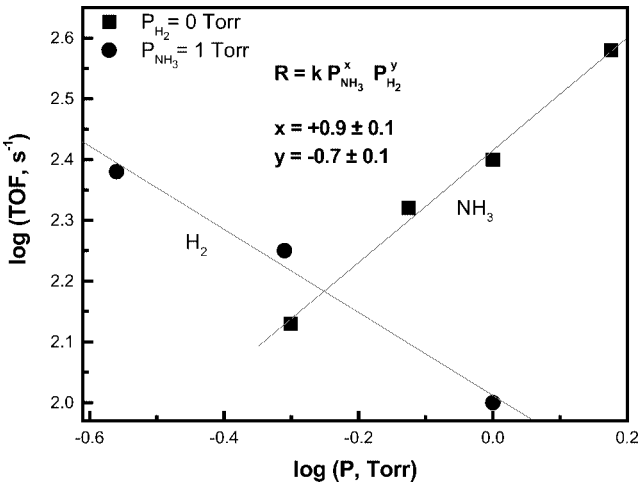

Figure 4. Specific ammonia decomposition rates as a function of ammonia (■) and hydrogen (●) partial pressures in logarithmic forms, $T = 775$ K.

To understand the effect of the exact role played by hydrogen we have carried out TPD experiments in the presence and absence of co-adsorbed hydrogen. Figure 5 shows TPD

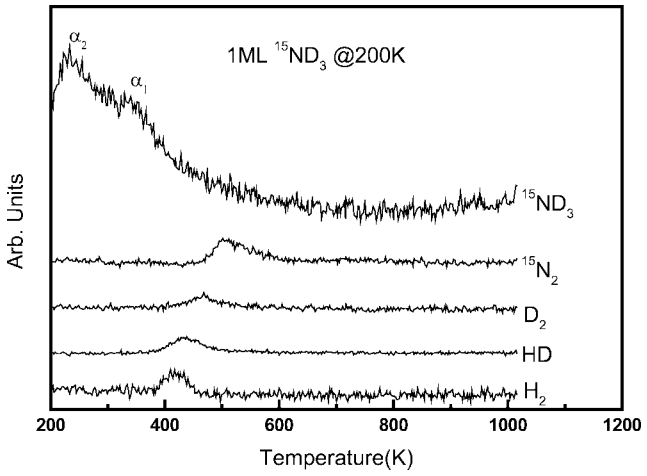

Figure 5. TPD spectra of m/e = 2, 3, 4, 21 and 30 from a 1 ML $^{15}ND_3$ adsorbed Ir(100) surface at 200 K.

spectra of m/e = 2, 3, 4, 21 and 30 of a monolayer $^{15}ND_3$ coverage at the adsorption temperature of 200 K. Desorption of molecular $^{15}ND_3$ (m/e = 21) is clearly evident with two distinct peaks whereas m/e = 3, 4 and 30 show a single desorption feature. According to our detailed study [21] these two desorption peaks (230 and 340 K, respectively) for ammonia (m/e = 21) can be assigned to α_1 and α_2 species due to chemisorbed ammonia, whereas the high temperature tail (400–500 K) of α_1 arises mainly from the recombinative reaction ($^{15}ND_2 + D \rightarrow {}^{15}ND_3$). Recombinative $^{15}N_2$ desorption ($^{15}N + {}^{15}N \rightarrow {}^{15}N_2$) occurs around 505 K. Interestingly, background H_2, HD and D_2 have different desorption temperature indicating clearly that ammonia decomposition occurs in a step-wise manner ($^{15}ND_3 \rightarrow {}^{15}ND_2 + D \rightarrow {}^{15}ND + D \rightarrow {}^{15}N + D$). The temperatures of desorption of HD and D_2 are higher than that of H_2 (adsorbed from background hydrogen), suggesting that the formation of HD and D_2 are reaction rate limited. From this set of data we can conclude that ammonia decomposes on Ir(100) in a stepwise manner and recombinative desorption is the rate-limiting step. The activation energy for recombinative $^{15}N_2$ desorption calculated using second-order reaction kinetics is ~63 kJ/mol, a value comparable to that of the total reaction activation energy.

Figure 6 (a) and (b) shows TPD spectra for m/e = 2, 3, 21 and 30 from 1 ML $^{15}ND_3$ covered surface with and without 1 ML co-adsorbed H_2. Distinct differences are evident with respect to the desorption temperatures when 1 ML hydrogen is co-adsorbed on the $^{15}ND_3$ preadsorbed surface. Two peaks (at *ca.* 400 and 465 K) are present in the TPD (figure 6(a)) of HD with the low-temperature peak aligned with the H_2 desorption peak suggesting that the origin of this feature is due to the isotopic exchange with the H atom generated after hydrogen exposure. The high-temperature HD desorption feature is from the decomposition of $^{15}ND_3$ and appears at a higher temperature compared to the surface with no adsorbed hydrogen. Also in figure 6(b) the α_1 and α_2 peaks of $^{15}ND_3$ as well as that of the $^{15}N_2$ desorption peak shift to higher temperatures relative to the surface with

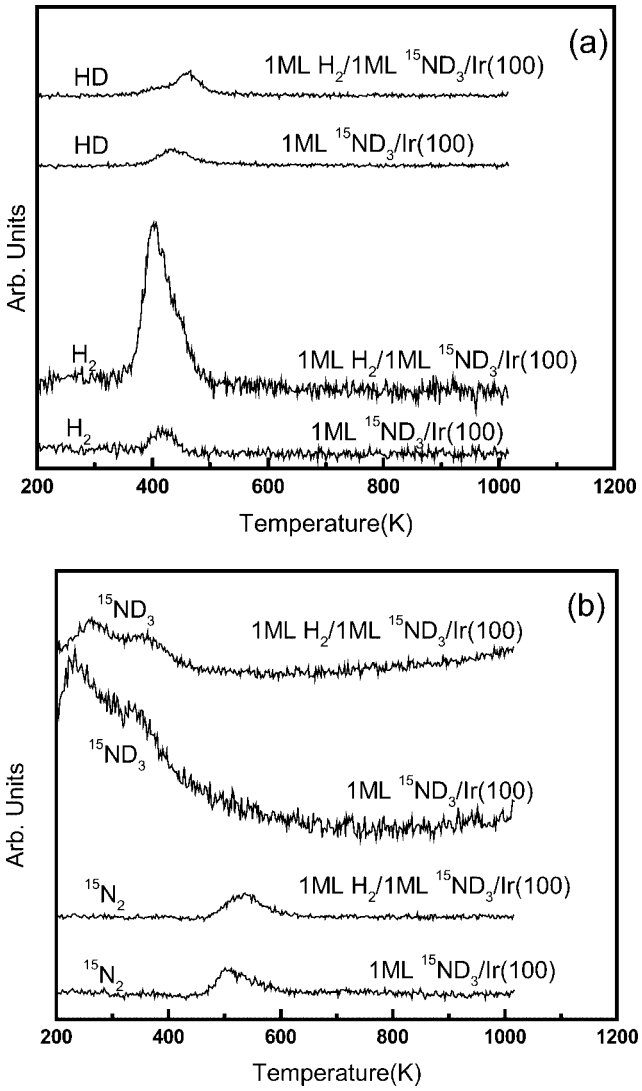

Figure 6. Comparison of the TPD spectra of (a) m/e = 2, 3 and (b) m/e = 21, 30 between Ir(100) surfaces with 1 ML $^{15}ND_3$ adsorbed and 1 ML H_2 adsorbed after 1 ML $^{15}ND_3$ adsorption at 200 K.

no co-adsorbed hydrogen. However, no change in the desorption temperature of H_2 is observed. This shift toward high temperature for desorption of HD, $^{15}ND_3$ and $^{15}N_2$ can be attributed to the effect of co-adsorbed hydrogen. In the presence of excess hydrogen atoms, the reverse reactions ($^{15}ND_x + D \rightarrow {}^{15}ND_{x+1}$, x = 0–2) are more favorable, therefore, the actual dissociation, *i.e.*, the forward reactions ($^{15}ND_{3-x} \rightarrow {}^{15}ND_{2-x} + D$, x = 0–2) occur at higher temperature where the H atom begins to desorb from the surface. This co-adsorption data clearly shows the effect of excess hydrogen on the surface and enables one to understand the negative order of the decomposition reaction found in the high-pressure experiments. The reason for the roll-over (at a given temperature) at a specific concentration of the hydrogen in the gas mixture (figure 1 (a) and (b)) may be understood by taking into account the enhanced rate of the reverse reactions (*i.e.*, $^{15}ND_x + D \rightarrow {}^{15}ND_{x+1}$, x = 0–2) due to the excess of D atoms.

4. Conclusions

(1) Ammonia decomposition occurs on an Ir(100) surface even under UHV condition and at adsorption temperatures as low as 200 K.

(2) Apparent reaction activation energy has been estimated to be 84 kJ/mol and is comparable to our high surface area Ir/Al_2O_3 data of ∼82 kJ/mol [19].

(3) The order of the reaction at 775 K has been estimated to be 0.9 and −0.7 for ammonia and hydrogen, respectively.

(4) Decomposition of NH_3 occurs in a stepwise manner where recombinative nitrogen desorption is the rate-determining step.

(5) The low value of recombinative desorption temperature indicates that there should not be any catalytic deactivation due to N atom poisoning or nitride formation under the actual catalytic conditions. In fact, our previous ammonia decomposition results [17] on high-surface-area Ir/Al_2O_3 show no sign of deactivation even after 6 h of time on stream reaction.

(6) The negative order of the reaction with respect to the hydrogen partial pressure can be understood by an enhancement of the reverse reactions ($NH_x + H \rightarrow NH_{x+1}$, $x = 0$–2) due to the increase in the dynamic surface coverage of H atoms arising form the dissociation of hydrogen in the gas mixture. Since the dynamic surface coverage is a function of surface temperature (expected to decrease with the increase in temperature) it is expected that at lower temperatures role-over should occur at lower partial pressure of hydrogen, *i.e.*, at lower ammonia conversion. As expected we have also seen the role-over at low ammonia conversion when hydrogen was co-introduced with ammonia in the gas mixture.

Acknowledgement

We acknowledge with pleasure the support of this work by the Department of Energy, Office of Basic Energy Sciences, Division of Chemical Sciences. TVC gratefully acknowledges the Link Foundation for the Link Energy Fellowship.

References

[1] J.R. Rostrup-Nielsen, in: *Catalytic Steam Reforming, Science and Engineering*, Vol. 5, eds. J.R. Anderson and M. Boudart (Springer, Berlin, 1984).
[2] J.N. Armor, Appl. Catal. 176 (1999) 159.
[3] T.V. Choudhary and D.W. Goodman, Catal. Lett. 59 (1999) 93.
[4] T.V. Choudhary and D.W. Goodman, J. Catal. 192 (2000) 316.
[5] T.V. Choudhary, C. Sivadinarayana, C. Chusuei, A. Klinghoffer and D.W. Goodman, J. Catal. 199 (2001) 9.
[6] T.V. Choudhary, C. Sivadinarayana, A. Klinghoffer and D.W. Goodman, Stud. Surf. Sci. Catal., in press.
[7] R. Metkemeijer and P. Achard, Int. J. Hydrogen Energy 19 (1994) 535; J. Power Sources 49 (1994) 271.
[8] R. Metkemeijer and P. Achard, J. Power Sources 49 (1994) 271.
[9] M. Asscher and Z. Rosenzweig, Surf. Sci. 225 (1990) 249.
[10] Y.K. Sun, Y. Q. Wang, C.B. Mullin and W.H. Weinberg, Langmuir 7 (1991) 1689;
W. Tsai and W. H. Weinberg, J. Phys. Chem. 91 (1987) 5302;
C. Egawa, T. Nishida, S. Naito and K. Tamaru, J. Chem. Soc. Faraday Trans. 80 (1984) 1595;
J.M. Bradeley, A. Hopkinson and D.A. King, Surf. Sci. 371 (1997) 255.
[11] W. Tsai, J.J. Vajo and W.H. Weinberg, J. Phys. Chem. 89 (1985) 4926;
J.J. Vajo, W. Tsai and W.H. Weinberg, J. Phys. Chem. 90 (1986) 6531; 89 (1985) 3243;
D.G. Loffler and L.D. Schmidt, Surf. Sci. 59 (1976) 195.
[12] C. Egawa, S. Naito and K. Tamaru, Surf. Sci. 131 (1983) 49;
M. Grossman and D.G. Loffler, J. Catal. 80 (1983) 188;
A.P.C. Reed and R.M. Lambert, J. Phys. Chem. 88 (1983) 1955.
[13] I.C. Bassignana, K. Wagemann, J. Kuppers and G. Ertl, Surf. Sci. 175 (1986) 22;
M. Huttinger and J. Kuppers, Surf. Sci. 130 (1983) L277;
D. Chrysostomou, J. Flowers and F. Zaera, Surf. Sci. 439 (1999) 34.
[14] G. Papapolymerou and V. Bontozoglou, J. Mol. Catal. A 120 (1997) 165.
[15] R.W. McCabe, J. Catal. 79 (1983) 445.
[16] E. Schmidt, *Hydrazine and its Derivatives, Preparation, Properties, Applications* (Wiley, New York, 1984).
[17] T.V. Choudhary and D.W. Goodman, J. Mol. Catal. 163 (2000) 9.
[18] C. Xu, W.S. Oh, D.Y. Kim and D.W. Goodman, J. Vac. Sci. Technol. A 15 (1997) 1261.
[19] T.V. Choudhary, C. Sivadinarayana and D.W. Gooodman, Catal. Lett. 72 (2001) 197.
[20] M. Grossman and D.G. Loffler, React. Kinet. Catal. Lett. 33 (1987) 87.
[21] A.K. Santra, B.K. Min, C.-W. Yi, T.V. Choudhary and D.W. Goodman, in preparation.